Eur. Phys. J. D **20**, 177–189 (2002)
DOI: 10.1140/epjd/e2002-00137-8

THE EUROPEAN PHYSICAL JOURNAL D

Two-color three-photon resonant excitation spectrum of strontium in the autoionization region

M. Yaseen[1], R. Ali[1], A. Nadeem[2], S.A. Bhatti[2], and M.A. Baig[1,a]

[1] Atomic and Molecular Physics Laboratory, Department of Physics, Quaid-i-Azam University, Islamabad 45320, Pakistan
[2] Applied Physics Division, PINSTECH, P.O. Box Nilore, Islamabad, Pakistan

Received 21 November 2001 / Received in final form 2 May 2002
Published online 19 July 2002 –

Abstract. We report new studies of the odd parity autoionizing Rydberg series of strontium attached to the $4d(^2\mathrm{D}_{3/2,5/2})$ ionic limits possessing $J = 1$–3 based on the two-color three photon resonant excitation technique in conjunction with an atomic beam apparatus. Using the $4d^2\ ^3\mathrm{P}_0$ intermediate levels, we have been able to record the autoionizing Rydberg series of $J = 1$ whereas, from the $4d^2\ ^3\mathrm{P}_2$ intermediate level the series of Rydberg levels possessing $J = 1$, 2 and 3 have been observed. The level assignments and the line shapes simulations of the autoionizing resonances have been made using the multichannel quantum defect theory.

PACS. 32.30.Jc Visible and ultraviolet spectra – 32.80.Rm Multiphoton ionization and excitation to highly excited states (e.g., Rydberg states)

1 Introduction

The spectra of alkaline earth atoms possessing filled s-subshells in the ground state are appropriate in understanding the correlation effects, energies and the stability properties of atoms. The doubly excited levels in the alkaline earth atoms can be considered as two independent one-electron systems yielding Rydberg series attached to each ionization threshold. Interactions among the Rydberg series converging to the highly excited ionization thresholds provide further insight in coupling with the underlying continua. This kind of work have become possible after the availability of tunable dye laser system and over the last decade there has been an explosion of new information on the highly excited autoionizing Rydberg atoms and their interchannel interactions ([1–4], and references therein).

Garton and Codling [5] were the first to report the odd parity $J = 1$ absorption spectra of the strontium atom in the ultraviolet region using a King type furnace and a three meter spectrograph. Rydberg series converging to the first ionization threshold and doubly excited series converging to the $4d(^2\mathrm{D}_{3/2,5/2})$ limits were photographed. Hudson *et al.* [6] reported the absorption cross-section of strontium in the autoionizing region from 164.6 to 202.8 nm at a resolution of 0.007 nm. Connerade *et al.* [7] reported the $J = 1$ Rydberg series converging to $4d(^2\mathrm{D}_{3/2,5/2})$ and $5p(^2\mathrm{P}_{1/2,3/2})$ ionic levels of strontium using synchrotron radiation as the continuum background source. Brown *et al.* [8] extended these studies to the wavelength range 140 nm using xenon and krypton lamps as the background sources and reported the doubly excited series built on the $4d$ and $5p$ ionic levels of strontium. Aymar [9] interpreted the doubly excited states in strontium by combining the eigen channel R-matrix method developed by Greene [10,11] with the multichannel quantum defect theory.

In the classical absorption spectroscopy, it was only possible to excite the odd parity $J = 1$ levels from the $5s^2\ ^1\mathrm{S}_0$ ground state. Multi-step and multi-photon spectroscopy had made it possible to study both the even and odd parity autoionizing spectra of different states of strontium ([3] and references therein). Kompitsas *et al.* [12] reported the odd parity $J = 3$ autoionizing spectrum below the $4d\ ^2\mathrm{D}_{5/2}$ threshold, using three photon non-resonant and two-step excitation technique in conjunction with an atomic beam apparatus. Subsequently, Kompitsas *et al.* [13] reported the even parity autoionizing spectrum for $J = 0$ below the $4d_{5/2}$ threshold employing two-step laser excitation from the ground state in an atomic beam apparatus. The importance of polarization techniques for the level assignment was inferred in situations where excited levels with more than one J-values were present. Goutis *et al.* [14] also used the same technique and further added the even parity transitions possessing $J = 1$ and 2 using $4d5p\ ^1\mathrm{P}_1$ intermediate level.

[a] e-mail: baig@qau.edu.pk

Jimoyiannis *et al.* [15] recorded the $4dn\ell$ even parity spectrum for $J = 0$–3 by the optogalvanic spectroscopic technique. These states were investigated using two-step laser excitation from the $4d5s$ metastable levels through the $4d5p\ ^3P_{0,1,2}$ intermediate levels. Farooqi *et al.* [16] observed the doubly excited states in the vicinity of the $4p\ ^2P_{3/2}$ threshold using the coherent four-wave mixing technique and a thermionic diode detector and the data were compared with the calculated spectra from the eigen-channel R-matrix method. In a subsequent paper, Jimoyiannis *et al.* [17] reported the $4dnd$ and $4dng$ $J = 3$–5 autoionizing Rydberg levels of strontium with two-step laser optogalvanic technique. Recently, Dai and Lu [18] reported the $5p_{1/2}nd$ ($J = 1$, 3) autoionizing states in strontium using an isolated core excitation scheme to supplement the earlier studies on the $5pn\ell$ ($\ell = 0$, 2) autoionizing states [19–22]. The photoionization cross-section of strontium in the autoionizing region, series terminating to the $4d(^2D_{3/2,5/2})$ and $5p(^2P_{1/2,3/2})$ limits were measured by Griesmann *et al.* [23] with a thermionic diode ion detector in conjunction with synchrotron radiation and the data were placed on an absolute scale.

Much of the early work is concentrated on studies of the even parity autoionizing Rydberg levels. In the present work, we report new investigations of the odd parity autoionizing Rydberg series of strontium attached to the $4d(^2D_{3/2,5/2})$ ionic limits possessing $J = 1$–3 using two-color three photon resonant excitation technique. The $J = 1$ levels have been observed from the $4d^2\ ^3P_0$ intermediate level whereas, $J = 1$, 2 and 3 Rydberg series are detected from the $4d^2\ ^3P_2$ intermediate level. The level assignments and the line shapes simulations of the autoionizing resonances are based on the multichannel quantum defect theory.

2 Experimental details

The experimental details are the same as described in our earlier paper [24]. Two Hänsch type dye lasers pumped by a common Nd:YAG (GCR-11) laser were used in conjunction with an atomic beam apparatus. The first dye laser (C-440 dye) was pumped by the third harmonics of the Nd:YAG laser, running at 10 Hz with a pulse width of 5–6 ns. This laser was focused by a 50 cm focal length quartz lens in the interaction region to populate the $4d^2\ ^3P_2$ or $4d^2\ ^3P_0$ intermediate levels through the two-photon excitation at 447 nm and 446 nm respectively. The second dye laser (DCM dye) was pumped by the second harmonics of the Nd:YAG laser to scan the region of interest from 660 to 620 nm. The line widths of both the lasers were $\approx$0.3 cm^{-1} and the pulse energy of the scanning dye laser was about 0.2 mJ.

A collimated beam of strontium vapor was produced by an oven that was resistively heated to a temperature in the range around 1 000 K. The atomic beam was passed through two stainless steel plates 1 cm apart where it intersected perpendicularly the two laser beams. The channeltron detector was placed above the 1 cm hole in the middle of the top plate which was covered with fine stainless steel mesh. About 0.5 volts were applied between the two plates to extract the ions and the signal was monitored by the Channeltron detector, operated at -1.8 kV DC.

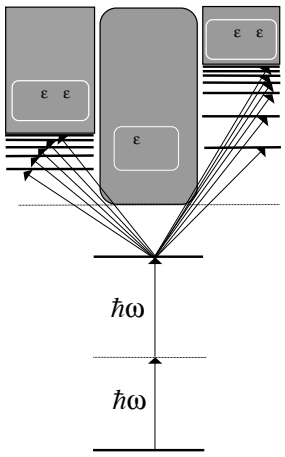

Fig. 1. Schematic energy level diagram of strontium showing the relevant participating levels in the excitation scheme. The ε_p and ε_f represent the continuum channels.

The first laser was focused into the strontium atomic beam and the second unfocused laser was overlapped with the first laser with a delay of about 3 ns. In order to find the intermediate transition from the first laser, it was scanned in the presence of the second laser. Once the first laser was tuned to the $4d^2\ ^3P_0$ or $4d^2\ ^3P_2$ level, its intensity was attenuated to avoid any direct photoionization. Keeping the first laser fixed the second laser was then scanned in the wavelength region from 670 to 620 nm.

A fraction of the second dye laser was injected into a neon hollow cathode lamp to record the optogalvanic spectra of neon and a small fraction of this laser beam passed through a 1.0 mm thick solid etalon to record the transmission fringes. Three box car averagers (SR 250) were used to monitor the ionization signal from the Channeltron detector, the optogalvanic spectra of neon and the etalon fringes. The data were processed *via* a SR-245 ADC interface on a 486 PC for further analysis and evaluation.

3 Results and discussion

The energy level diagram of strontium showing the relevant levels is shown in Figure 1. The first step is a two photon excitation process, therefore, from the $5s^2\ ^1S_0$ ground state the even parity $4d^2\ ^3P_0$ or $^3P_2$ levels are accessible that lie at 44 525.88 cm^{-1} and 44 729.67 cm^{-1} respectively [25]. From the $4d^2\ ^3P_0$ intermediate level, the excited $4d(^2D_{3/2,5/2})n\ell$ levels with $J = 1$ are observed *via* single photon excitation. Using $4d^2\ ^3P_2$ as an intermediate level, we have observed the $4d(^2D_{3/2,5/2})n\ell$ Rydberg series possessing $J = 1$, 2 and 3. The excited levels are designated in the jK-coupling scheme which is more appropriate to represent the doubly excited levels in strontium as already remarked by Hudson *et al.* [6].

In this coupling scheme $[\{(\ell_1, s_1)j, \ell_2\}K, s_2]J$, the angular momentum quantum number j of the core electron $(4d_j,\ j = 3/2,\ 5/2)$ couples with the orbital angular momentum ℓ_2 of the excited electron to form K quantum number. K is then weakly coupled to the spin s_2 of the excited electron to yield the total J-value. The levels are designated as $[K]_J$.

The possible $4dn\ell$ ($\ell = 1$ and $\ell = 3$) Rydberg series converging to the $4d(^2\mathrm{D}_{3/2})$ ionization threshold at 60 488.0 cm^{-1} are:

$4d^2\ {}^3\mathrm{P}_2 \rightarrow 4d(^2\mathrm{D}_{3/2})np\,[1/2]_1$ $\quad$ $4d^2\ {}^3\mathrm{P}_2 \rightarrow 4d(^2\mathrm{D}_{3/2})nf\,[3/2]_{1,2}$

$4d^2\ {}^3\mathrm{P}_2 \rightarrow 4d(^2\mathrm{D}_{3/2})np\,[3/2]_{1,2}$ $\quad$ $4d^2\ {}^3\mathrm{P}_2 \rightarrow 4d(^2\mathrm{D}_{3/2})nf\,[5/2]_{2,3}$

$4d^2\ {}^3\mathrm{P}_2 \rightarrow 4d(^2\mathrm{D}_{3/2})np\,[5/2]_{2,3}$ $\quad$ $4d^2\ {}^3\mathrm{P}_2 \rightarrow 4d(^2\mathrm{D}_{3/2})nf\,[7/2]_3$

and the Rydberg series converging to the $4d$ $(^2\mathrm{D}_{5/2})$ ionization limit at 60 768.34 cm^{-1} are:

$4d^2\ {}^3\mathrm{P}_2 \rightarrow 4d(^2\mathrm{D}_{5/2})np\,[3/2]_{1,2}$ $\quad$ $4d^2\ {}^3\mathrm{P}_2 \rightarrow 4d(^2\mathrm{D}_{5/2})nf\,[1/2]_1$

$4d^2\ {}^3\mathrm{P}_2 \rightarrow 4d(^2\mathrm{D}_{5/2})np\,[5/2]_{2,3}$ $\quad$ $4d^2\ {}^3\mathrm{P}_2 \rightarrow 4d(^2\mathrm{D}_{5/2})nf\,[3/2]_{1,2}$

$4d^2\ {}^3\mathrm{P}_2 \rightarrow 4d(^2\mathrm{D}_{5/2})np\,[7/2]_3$ $\quad$ $4d^2\ {}^3\mathrm{P}_2 \rightarrow 4d(^2\mathrm{D}_{5/2})nf\,[5/2]_{2,3}$

$4d^2\ {}^3\mathrm{P}_2 \rightarrow 4d(^2\mathrm{D}_{5/2})nf\,[7/2]_3$.

Twenty one different Rydberg series may arise converging to the $4d(^2\mathrm{D}_{3/2,5/2})$ ionic levels. According to the dipole selection rules in the jK coupling scheme, the most probable transitions will be those which obey the $\Delta j_1 = 0$ and $\Delta K = \Delta J = +\Delta\ell$ selection rules. Accordingly, a number of series will be either absent or will be of very low intensity.

Since all these observed levels lie above the first ionization threshold, the interaction of these channels develops an autoionization behavior with the corresponding open channels $\varepsilon\ell$ of the first ionization threshold $5s\ {}^2\mathrm{S}_{1/2}$. This interaction is visible from the line shapes and intensities of the observed spectral lines.

Since the observed spectrum consists of $J = 1$, 2 and 3 levels, therefore transition energies have been matched with the existing data for the $J = 1$ levels reported by Garton and Codling [5] and Brown *et al.* [8]. The $J = 3$ data are compared with that of Kompitsas *et al.* [12] who employed the multi-step laser excitation scheme using the $5p^2\ {}^1\mathrm{D}_2$ as the intermediate level. The remaining lines belong to the $J = 2$ channels. The observed lines are classified to different groups by looking at their line shapes, widths, intensities and the quantum defect pertaining to different series using the Rydberg relation:

$$E_n = IP - \frac{Ry}{(n - \delta_\ell)^2} \tag{1}$$

where E_n is the term energy, IP is the ionization potential, $Ry = 109\,736.8$ cm^{-1} is the mass corrected Rydberg constant of strontium and δ_ℓ is the quantum defect. We present absolute energies of all the observed Rydberg series in Table 1 which have been determined by adding the laser excitation energies to the energies of the intermediate levels: $4d^2\ {}^3\mathrm{P}_0$ at 44 525.88 cm^{-1} and $4d^2\ {}^3\mathrm{P}_2$ at 44 729.67 cm^{-1} [25]. This table contains effective quantum numbers with respect to $d_{3/2}$ and $d_{5/2}$ limits and the widths of the autoionizing resonances. The estimated experimental uncertainty is about ± 0.5 cm^{-1}.

For the $J = 1$ spectrum, Garton and Codling [5] observed six series, two np and one nf series to the $4d\ {}^2\mathrm{D}_{3/2}$ limit and one np and two nf series to the $4d\ {}^2\mathrm{D}_{5/2}$ limit. Garton and Codling [5] used LS as well as jK coupling designations for the lower members of the series. The $4d(^2\mathrm{D}_{5/2})np\ {}^1\mathrm{P}_1\ [3/2]_1$ was the dominating and strongly autoionizing whereas, the $4d(^2\mathrm{D}_{3/2})np\ {}^3\mathrm{P}_1\ [3/2]_1$ and $4d(^2\mathrm{D}_{3/2})np\ {}^3\mathrm{D}_1\ [1/2]_1$ were of relatively narrow line widths reflecting their weak coupling with the ionization continuum. The $4d(^2\mathrm{D}_{3/2,5/2})nf$ series remains much sharper as compared to the $4d(^2\mathrm{D}_{3/2,5/2})np$ series as they do not couple with the adjacent continua. However, a change in the line intensities and autoionization line shapes have been observed below the $4d\ {}^2\mathrm{D}_{3/2}$ limit. The variation in the line intensities is also an indication of the change of the coupling from LS to jK or jj with increasing principal quantum number n. Brown *et al.* [8] observed this complicated spectrum at a much higher dispersion and resolution who reported only the level energies and effective quantum numbers without level assignments. The series attached to the $4d(^2\mathrm{D}_{5/2})$ limit were assigned by Hudson *et al.* [6] as $4d(^2\mathrm{D}_{5/2})np\ [3/2]_1\ {}^1\mathrm{P}_1$ and $4d(^2\mathrm{D}_{5/2})nf\ [3/2]_1\ {}^1\mathrm{P}_1$ with effective quantum numbers $\nu_{5/2}\ (\mathrm{mod}\ 1) = 0.31$ and 0.74 respectively. The autoionizing resonances observed by Brown *et al.* [8] between the $4d_{3/2}$ and $4d_{5/2}$ thresholds possess $\nu_{5/2}\ (\mathrm{mod}\ 1) = 0.31$ and 0.74 respectively. Aymar [9] assigned the series with $\nu_{5/2}\ (\mathrm{mod}\ 1) = 0.15$, 0.35 and 0.65 as $4d_{5/2}np_{3/2}$, $4d_{5/2}nf_{5/2}$ and $4d_{5/2}nf_{7/2}$ respectively based on the eigenchannel R-matrix calculations of the photo-absorption spectrum of strontium.

For the $J = 3$ odd parity spectra of strontium *via* the $4p^2\ {}^1\mathrm{D}_2$ intermediate level Kompitsas *et al.* [12] reported autoionizing resonances between the $5s$ and $4d$ thresholds. The spectra were interpreted with the help of theoretical calculations based on the R-matrix method combined with multi-channel quantum defect theory. The experimentally observed transitions in the region 53 290 cm^{-1} to 59 142 cm^{-1} were assigned as $4d(^2\mathrm{D}_{3/2,5/2})np\ (7 \le n \le 11)$, $nf\ (4 \le n \le 9)$ and $nh\ (6 \le n \le 9)$ in comparison with theoretical calculations.

In Figure 2a we show the spectrum of strontium excited from the $4d^2\ {}^3\mathrm{P}_0$ intermediate level covering the energy region from 60 150 to 59 900 cm^{-1}. Since only the levels with $J = 1$ are accessible the level assignments are straightforward by comparing our data with that of Garton and Codling [5] and Brown *et al.* (1974). It is worth noting that only levels built on the $4d\ {}^2\mathrm{D}_{3/2}$ parent ion level are apparent and the $4d\ {}^2\mathrm{D}_{5/2}\ np$ ($n = 14$ and 15) lines are very weak. Incidentally, there is a very strong line at 59 980 cm^{-1} (scanning laser energy = 15 462.7 cm^{-1}) which is attributed to the sequential excitation from the $4s5p\ {}^1\mathrm{P}_1$ resonance level to the $5p^2\ {}^1\mathrm{S}_0$ level (term energy = 37 160.5 cm^{-1}).

Table 1. Level energies and widths of the odd parity $J = 1$, 2 and 3 series converging to the $4d\ ^2\mathrm{D}_{3/2,5/2}$, limits excited from the $4d^2\ ^3\mathrm{P}_2$ intermediate level.

Level energy (cm^{-1})	Assignment	ν_1 ($^2\mathrm{D}_{3/2}$)	ν_2 ($^2\mathrm{D}_{5/2}$)	Width (cm^{-1})	Appearance
59 873.8	$^2\mathrm{D}_{5/2}11f\ [7/2]_3$	13.363	11.076	1.1	m
59 902.2	$^2\mathrm{D}_{5/2}14p\ [3/2]_2$	13.658	11.255	0.6	m
59 907.6	$^2\mathrm{D}_{5/2}14p\ [3/2]_1$	13.744	11.285	2.8	s
59 920.0	$^2\mathrm{D}_{5/2}14p\ [5/2]_{2,3}$	13.894	11.373	3.9	m
59 924.7	$^2\mathrm{D}_{3/2}14f\ [3/2]_1$	13.953	11.405	1.3	w
59 930.0	$^2\mathrm{D}_{5/2}14p\ [7/2]_3$	14.020	11.441	2.2	s
59 947.3	$^2\mathrm{D}_{3/2}17p\ [3/2]_1$	14.245	11.561	0.7	w
59 967.8	$^2\mathrm{D}_{5/2}12f\ [5/2]_{2,3}$	14.519	11.708	7.1	w
59 985.3	$^2\mathrm{D}_{3/2}15f\ [3/2]_1$	14.771	11.839	0.9	w
59 992.9	$^1\mathrm{P}_1 - 5p^2\ ^1\mathrm{D}_2$				vs
60 001.6	$^2\mathrm{D}_{5/2}12f\ [3/2]_2$	14.989	11.952	0.9	w
60 014.4	$^2\mathrm{D}_{5/2}12f\ [7/2]_3$	15.216	12.064	1.9	s
60 018.7	$^2\mathrm{D}_{3/2}18p\ [3/2]_1$	15.286	12.099	1.7	Overlapped
60 025.6		15.399	12.155	1.4	w
60 036.0	$^2\mathrm{D}_{5/2}15p\ [3/2]_2$	15.58	12.249	0.8	w
60 040.6	$^2\mathrm{D}_{5/2}15p\ [3/2]_1$	15.642	12.278	2.0	s
60 051.7	$^2\mathrm{D}_{5/2}15p\ [5/2]_{2,3}$	15.852	12.374	2.8	m
60 055.6	$^2\mathrm{D}_{3/2}16f\ [3/2]_1$	15.915	12.406	1.3	m
60 059.6	$^2\mathrm{D}_{5/2}15p\ [7/2]_3$	15.998	12.443	5.7	s
60 072.6	$^2\mathrm{D}_{3/2}19p\ [3/2]_1$	16.247	12.599	1.4	w
60 085.4	$^2\mathrm{D}_{5/2}13f\ [5/2]_{2,3}$	16.502	12.676	5.9	s
60 098.9	$^2\mathrm{D}_{3/2}17f\ [3/2]_1$	16.788	12.804		Overlapped
60 108.7	$^2\mathrm{D}_{5/2}13f\ [3/2]_2$	17.001	12.898	1.7	w
60 122.2	$^2\mathrm{D}_{3/2}20p\ [3/2]_1$	17.313	13.032	1.0	sh
60 123.5	$^2\mathrm{D}_{5/2}13f\ [7/2]_3$	17.342	13.045	0.8	s
60 140.8	$^2\mathrm{D}_{5/2}16p\ [3/2]_2$	17.769	13.224	1.1	Overlapped
60 143.1	$^2\mathrm{D}_{3/2}18f\ [3/2]_1$	17.837	13.248	2.0	s
60 150.3	$^2\mathrm{D}_{5/2}16p\ [7/2]_3$	18.016	13.325	2.0	s
60 155.3	$^2\mathrm{D}_{5/2}16p\ [5/2]_{2,3}$	18.151	13.379	1.6	w
60 159.0	$^2\mathrm{D}_{3/2}21p\ [3/2]_1$	18.252	13.421	0.2	w
60 171.1	$^2\mathrm{D}_{5/2}14f\ [5/2]_{2,3}$	18.596	13.554	5.9	s
60 183.0		18.958	13.692	0.7	w
60 185.0	$^2\mathrm{D}_{3/2}18f\ [3/2]_1$	19.020	13.713	1.7	s
60 191.9	$^1\mathrm{P}_1 - 5\mathrm{P}^2\ ^1\mathrm{S}_0$				vs
60 194.9	$^2\mathrm{D}_{5/2}14f\ [5/2]_2$	19.338	13.834	1.1	w
60 211.4		19.906	14.037	1.0	s
60 214.5	$^2\mathrm{D}_{5/2}14f\ [7/2]_3$	20.013	14.075	1.7	m
60 227.0	$^2\mathrm{D}_{5/2}17p\ [3/2]_2$	20.494	14.232	0.5	s
60 230.5	$^2\mathrm{D}_{5/2}17p\ [3/2]_1$	20.557	14.285		Overlapped
60 235.5	$^2\mathrm{D}_{5/2}17p\ [5/2]_{2,3}$	20.830	14.352	2.2	s
60 239.0	$^2\mathrm{D}_{5/2}17p\ [7/2]_3$	20.975	14.397	1.5	s
60 252.1	$^2\mathrm{D}_{5/2}15f\ [5/2]_{2,3}$	21.549	14.580	4.8	m
60 261.0		21.969	14.707	2.4	m
60 266.0	$^2\mathrm{D}_{5/2}15f\ [3/2]_2$	22.218	14.781	2.4	s
60 268.2	$^2\mathrm{D}_{5/2}15f\ [3/2]_2$	22.327	14.813	0.6	w
60 282.9	$^2\mathrm{D}_{5/2}15f\ [7/2]_3$	23.110	15.037	1.2	vs
60 299.4	$^2\mathrm{D}_{5/2}18p\ [3/2]_2$		15.247	5.5	s
60 301.2	$^2\mathrm{D}_{5/2}18p\ [3/2]_1$		15.327	1.3	m
60 307.9	$^2\mathrm{D}_{5/2}18p\ [5/2]_{2,3}$		15.438	3.7	s
60 312.5	$^2\mathrm{D}_{5/2}18p\ [7/2]_3$		15.516	1.3	m
60 317.9	$^2\mathrm{D}_{5/2}16f\ [5/2]_{2,3}$		15.609	2.7	s
60 325.3			15.738	0.9	m
60 328.3	$^2\mathrm{D}_{5/2}16f\ [3/2]_2$		15.793	1.6	m
60 337.8			15.958	0.4	w
60 340.7	$^2\mathrm{D}_{5/2}16f\ [7/2]_3$		16.023	1.8	s
60 347.5			16.148	1.5	w

Table 1. *Continued.*

Level energy (cm^{-1})	Assignment	ν_1 ($^2D_{3/2}$)	ν_2 ($^2D_{5/2}$)	Width (cm^{-1})	Appearance
60 352.7	$^2D_{5/2}19p\ [3/2]_2$		16.249	2.6	s
60 356.1	$^2D_{5/2}19p\ [3/2]_1$		16.315	1.0	w
60 357.8			16.350	1.0	m
60 363.2	$^2D_{5/2}19p\ [5/2]_{2,3}$		16.458	3.2	s
60 366.1	$^2D_{5/2}19p\ [7/2]_3$		16.518	0.3	m
60 367.4			16.587	1.7	s
60 376.2	$^2D_{5/2}17f\ [5/2]_{2,3}$		16.728	2.1	m
60 381.7	$^2D_{5/2}17f\ [3/2]_2$		16.847	1.2	w
60 389.4	$^2D_{5/2}17f\ [7/2]_3$		17.018	1.1	s
60 393.0			17.099	1.3	s
60 399.5	$^2D_{5/2}20p\ [5/2]_2$		17.249	2.3	s
60 402.1	$^2D_{5/2}20p\ [3/2]_1$		17.310	2.3	s
60 403.9	$^2D_{5/2}20p\ [5/2]_2$		17.335	2.0	m
60 406.1	$^2D_{5/2}20p\ [5/2]_3$		17.411	2.7	s
60 408.1	$^2D_{5/2}20p\ [7/2]_3$		17.502	1.3	w
60 412.0			17.549		
60 413.7			17.590	1.2	s
60 416.1	$^2D_{5/2}18f\ [5/2]_2$		17.650		
60 417.5	$^2D_{5/2}18f\ [5/2]_3$		17.686	1.4	m
60 421.0			17.772	1.2	w
60 423.5	$^2D_{5/2}18f\ [3/2]_2$		17.837	1.3	w
60 426.3			17.915	0.9	w
60 430.7	$^2D_{5/2}18f\ [7/2]_3$		18.028	0.9	s
60 438.8	$^2D_{5/2}21p\ [3/2]_2$		18.245	2	m
60 440.3	$^2D_{5/2}21p\ [3/2]_1$		18.289		
60 442.5	$^2D_{5/2}21p\ [5/2]_2$		18.354	0.3	m
60 445.0	$^2D_{5/2}21p\ [5/2]_3$		18.422		
60 448.0	$^2D_{5/2}21p\ [7/2]_3$		18.507		s
60 449.2			18.574		s
60 453.6	$^2D_{5/2}19f\ [5/2]_2$		18.674		
60 455.6			18.731		
60 459.9	$^2D_{5/2}19f\ [3/2]_2$		18.830		
60 461.2			18.902		
60 465.0	$^2D_{5/2}19f\ [7/2]_3$		19.021	1.6	s
60 465.9			19.047		
60 467.9			19.113		
60 471.7	$^2D_{5/2}22p\ [3/2]_2$		19.235	2.1	s
60 473.1	$^2D_{5/2}22p\ [3/2]_1$		19.279		
60 475.1	$^2D_{5/2}22p\ [5/2]_2$		19.343	0.4	s
60 477.3	$^2D_{5/2}22p\ [5/2]_3$		19.463	0.5	s
60 481.6			19.562	0.3	s
60 484.4	$^2D_{5/2}20f\ [5/2]_2$		19.659		
60 487.0			19.750		
60 489.1	$^2D_{5/2}20f\ [3/2]_2$		19.822		
60 494.4			20.016		
60 495.1	$^2D_{5/2}20f\ [7/2]_3$		20.041		
60 495.8			20.065		
60 497.1			20.116		
60 500.5	$^2D_{5/2}23p\ [3/2]_2$		20.240		
60 501.8	$^2D_{5/2}23p\ [3/2]_1$		20.292		
60 504.0	$^2D_{5/2}23p\ [5/2]_2$		20.376		
60 505.4	$^2D_{5/2}23p\ [5/2]_3$		20.426		
60 507.1	$^2D_{5/2}23p\ [7/2]_3$		20.493		
60 508.2			20.538		
60 511.1	$^2D_{5/2}21f\ [5/2]_2$		20.656		
60 512.3	$^2D_{5/2}21f\ [5/2]_3$		20.710		
60 515.1	$^2D_{5/2}21f\ [3/2]_2$		20.815		

Table 1. *Continued.*

Level energy (cm^{-1})	Assignment	ν_1 ($^2D_{3/2}$)	ν_2 ($^2D_{5/2}$)	Width (cm^{-1})	Appearance
60 519.7			21.009		
60 520.5	$^2D_{5/2}21f\ [7/2]_3$		21.040		
60 522.0			21.105		
60 525.3	$^2D_{5/2}24p\ [3/2]_2$		21.243		
60 526.4	$^2D_{5/2}24p\ [3/2]_1$		21.298		
60 527.8	$^2D_{5/2}24p\ [5/2]_2$		21.375		
60 528.9	$^2D_{5/2}24p\ [7/2]_3$		21.423		
60 530.8	$^2D_{5/2}24p\ [7/2]_3$		21.496		
60 532.5			21.571		
60 534.6	$^2D_{5/2}22f\ [5/2]_2$		21.667		
60 535.5	$^2D_{5/2}22f\ [5/2]_3$		21.710		
60 536.9			21.776		
60 538.4	$^2D_{5/2}22f\ [3/2]_2$		21.847		
60 542.0			22.019		
60 542.7	$^2D_{5/2}22f\ [7/2]_3$		22.053		
60 544.3			22.129		
60 546.7	$^2D_{5/2}25p\ [3/2]_2$		22.248		
60 548.1	$^2D_{5/2}25p\ [3/2]_1$		22.321		
60 548.5			22.335		
60 548.7	$^2D_{5/2}25p\ [5/2]_2$		22.371		
60 549.9	$^2D_{5/2}25p\ [5/2]_2$		22.414		
60 551.5	$^2D_{5/2}25p\ [7/2]_3$		22.495		
60 552.4			22.557		
60 554.5	$^2D_{5/2}23f\ [5/2]_{2,3}$		22.654		
60 556.6			22.764		
60 557.2	$^2D_{5/2}23f\ [3/2]_2$		22.797		
60 560 .8			22.992		
60 561.6	$^2D_{5/2}23f\ [7/2]_3$		23.040		
60 562.9			23.114		
60 563.9			23.171		
60 564.8	$^2D_{5/2}26p\ [3/2]_2$		23.220		
60 566.5	$^2D_{5/2}26p\ [3/2]_1$		23.318		
60 567.4	$^2D_{5/2}26p\ [5/2]_2$		23.371		
60 568.3	$^2D_{5/2}26p\ [5/2]_3$		23.424		
60 569.8	$^2D_{5/2}26p\ [7/2]_3$		23.508		
60 572.6	$^2D_{5/2}24f\ [5/2]_{2,3}$		23.679		
60 574.0			23.763		
60 577.6			23.986		
60 578.5	$^2D_{5/2}24f\ [7/2]_3$		24.042		
60 579.4			24.101		
60 580.6			24.177		
60 581.4	$^2D_{5/2}27p\ [3/2]_2$		24.229		
60 582.8	$^2D_{5/2}27p\ [3/2]_1$		24.319		
60 584.0	$^2D_{5/2}27p\ [5/2]_2$		24.382		
60 584.9	$^2D_{5/2}27p\ [5/2]_3$		24.459		
60 585.9	$^2D_{5/2}27p\ [7/2]_3$		24.527		
60 588.2	$^2D_{5/2}25f\ [5/2]_{2,3}$		24.679		
60 589.6			24.776		
60 590.6	$^2D_{5/2}25f\ [3/2]_2$		24.850		
60 593.1			25.024		
60 593.6	$^2D_{5/2}25f\ [7/2]_3$		25.059		
60 594.8			25.148		
60 595.6			25.203		
60 596.3	$^2D_{5/2}28p\ [3/2]_2$		25.258		
60 597.6	$^2D_{5/2}28p\ [3/2]_1$		25.349		
60 598.1	$^2D_{5/2}28p\ [5/2]_{2,3}$		25.386		
60 599.0	$^2D_{5/2}28p\ [5/2]_3$		25.454		

Table 1. *Continued.*

Level energy (cm^{-1})	Assignment	ν_1 ($^2D_{3/2}$)	ν_2 ($^2D_{5/2}$)	Width (cm^{-1})	Appearance
60 600.2	$^2D_{5/2}28p\ [7/2]_3$		25.548		
60 601.9	$^2D_{5/2}26f\ [5/2]_{2,3}$		25.677		
60 604.0	$^2D_{5/2}26f\ [3/2]_2$		25.837		
60 606.1			26.010		
60 606.6	$^2D_{5/2}26f\ [7/2]_3$		26.049		
60 607.5			26.120		
60 608.4			26.193		
60 609.2	$^2D_{5/2}29p\ [3/2]_2$		26.257		
60 610.2	$^2D_{5/2}29p\ [3/2]_1$		26.345		
60 610.7	$^2D_{5/2}29p\ [5/2]_2$		26.385		
60 611.5	$^2D_{5/2}29p\ [5/2]_2$		26.447		
60 612.2	$^2D_{5/2}29p\ [7/2]_3$		26.513		
60 614.4	$^2D_{5/2}27f\ [5/2]_{2,3}$		26.696		
60 615.7	$^2D_{5/2}27f\ [3/2]_2$		26.809		
60 618.0			27.021		
60 618.3	$^2D_{5/2}27f\ [7/2]_3$		27.046		
60 619.3			27.132		
60 619.9			27.193		
60 620.5	$^2D_{5/2}30p\ [3/2]_2$		27.246		
60 622.3	$^2D_{5/2}30p\ [5/2]_{2,3}$		27.414		
60 623.9			27.564		
60 624.3	$^2D_{5/2}28f\ [5/2]_{2,3}$		27.601		
60 624.4			27.613		
60 625.8			27.748		
60 626.7			27.775		
60 628.7	$^2D_{5/2}28f\ [7/2]_3$		28.029		
60 629.5			28.113		
60 631.1			28.278		
60 631.5	$^2D_{5/2}31p\ [3/2]_1$		28.319		
60 632.3			28.401		
60 633.3	$^2D_{5/2}31p\ [7/2]_3$		28.538		
60 634.0			28.583		
60 635.7	$^2D_{5/2}29f\ [5/2]_{2,3}$		28.767		
60 636.3	$^2D_{5/2}29f\ [3/2]_2$		28.825		
60 638.3	$^2D_{5/2}29f\ [7/2]_3$		29.050		
60 639.1			29.139		
60 640.0	$^2D_{5/2}32p\ [3/2]_2$		29.241		
60 641.1	$^2D_{5/2}32p\ [5/2]_2$		29.372		
60 641.8	$^2D_{5/2}32p\ [5/2]_3$		29.451		
60 642.5	$^2D_{5/2}32p\ [7/2]_3$		29.535		
60 643.7	$^2D_{5/2}30f\ [5/2]_{2,3}$		29.670		
60 644.8	$^2D_{5/2}30f\ [3/2]_2$		29.800		
60 646.9	$^2D_{5/2}30f\ [7/2]_3$		30.066		
60 647.5			30.135		
60 648.6	$^2D_{5/2}33p\ [3/2]_2$		30.269		
60 648.8	$^2D_{5/2}33p\ [3/2]_1$		30.294		
60 649.1	$^2D_{5/2}33p\ [5/2]_2$		30.377		
60 650.2	$^2D_{5/2}33p\ [7/2]_3$		30.481		
60 651.5			30.643		
60 652.0			30.709		
60 654.7	$^2D_{5/2}31f\ [7/2]_3$		31.077		
60 655.5			31.179		
60 656.2	$^2D_{5/2}34p\ [3/2]_2$		31.276		
60 656.5	$^2D_{5/2}34p\ [5/2]_2$		31.372		
60 657.5	$^2D_{5/2}34p\ [5/2]_3$		31.460		
60 657.9			31.526		
60 658.5	$^2D_{5/2}32f\ [5/2]_{2,3}$		31.611		

Table 1. *Continued.*

Level energy (cm^{-1})	Assignment	ν_1 ($^2D_{3/2}$)	ν_2 ($^2D_{5/2}$)	Width (cm^{-1})	Appearance
60 659.1			31.700		
60 660.1			32.443		
60 661.5			32.050		
60 661.8	$^2D_{5/2}32f\ [7/2]_3$		32.087		
60 662.6			32.221		
60 662.6	$^2D_{5/2}35p\ [3/2]_2$		32.260		
60 663.2	$^2D_{5/2}35p\ [3/2]_1$		32.304		
60 663.4	$^2D_{5/2}35p\ [5/2]_2$		32.343		
60 664.7	$^2D_{5/2}35p\ [7/2]_3$		32.545		
60 664.8			32.371		
60 665.8	$^2D_{5/2}33f\ [5/2]_{2,3}$		32.716		
60 667.9			33.035		
60 668.5	$^2D_{5/2}33f\ [7/2]_3$		33.151		
60 669.3	$^2D_{5/2}36p\ [3/2]_1$		33.291		
60 670.4	$^2D_{5/2}36p\ [7/2]_3$		33.469		
60 671.1	$^2D_{5/2}34f\ [5/2]_{2,3}$		33.589		
60 673.9	$^2D_{5/2}34f\ [7/2]_3$		34.093		
60 674.5			34.198		
60 674.7	$^2D_{5/2}37p\ [3/2]_2$		34.222		
60 674.9	$^2D_{5/2}37p\ [3/2]_1$		34.277		
60 675.9	$^2D_{5/2}37p\ [5/2]_3$		34.447		
60 676.4			34.555		
60 677.5	$^2D_{5/2}35f\ [5/2]_{2,3}$		34.750		
60 679.0	$^2D_{5/2}35f\ [7/2]_3$		35.049		
60 679.8			35.197		
60 680.0	$^2D_{5/2}38p\ [3/2]_2$		35.253		
60 680.4	$^2D_{5/2}38p\ [3/2]_1$		35.318		
60 680.9	$^2D_{5/2}38p\ [5/2]_3$		35.432		
60 681.4	$^2D_{5/2}38p\ [7/2]_3$		35.537		
60 682.4	$^2D_{5/2}36f\ [5/2]_{2,3}$		5.728		
60 683.9	$^2D_{5/2}36f\ [7/2]_3$		36.046		
60 684.6			36.206		
60 685.0	$^2D_{5/2}39p\ [3/2]_2$		36.282		
60 685.3	$^2D_{5/2}39p\ [5/2]_2$		36.357		
60 686.2	$^2D_{5/2}39p\ [7/2]_3$		36.536		
60 688.5	$^2D_{5/2}37f\ [7/2]_3$		37.081		
60 689.4	$^2D_{5/2}40p\ [3/2]_2$		37.274		
60 692.8	$^2D_{5/2}39f\ [7/2]_3$		38.121		
60 693.3	$^2D_{5/2}41p\ [3/2]_2$		38.249		
60 693.7	$^2D_{5/2}41p\ [5/2]_2$		38.345		
60 694.3	$^2D_{5/2}41p\ [7/2]_3$		38.487		
60 694.9			38.646		
60 696.6	$^2D_{5/2}42p\ [7/2]_3$		39.106		
60 697.3	$^2D_{5/2}42p\ [3/2]_2$		39.306		
60 697.9	$^2D_{5/2}42p\ [5/2]_3$		39.462		
60 700.5	$^2D_{5/2}43p\ [3/2]_2$		40.205		
60 701.3	$^2D_{5/2}43p\ [5/2]_3$		40.456		
60 701.7	$^2D_{5/2}43p\ [7/2]_3$		40.575		

vs: very strong, s: strong, ms: medium strong, m: medium, w: weak, sh: shoulder 1.

Figure 2b shows the spectrum of strontium pertaining to $5dn\ell$ configurations excited from the $4d^2\ ^3P_2$ intermediate level and covering the same energy as in Figure 2a. We have particularly selected this region to display the relative intensities of the levels attached to both the $4d\ ^2D_{3/2}$ and $^2D_{5/2}$ ionic limits. Since the assignment for the $J = 1$ levels are well established (Garton and Codling, 1968), all the additional levels possess either $J = 2$ or $J = 3$. The observed $4d(^2D_{3/2})np\ [3/2]_1$ ($17 \leq n \leq 20$) are sharper and nearly 5 times lower in intensity as compared to the corresponding $4d(^2D_{5/2})np\ [3/2]_1$ series. Surprisingly, no other series built on the $4d_{3/2}$

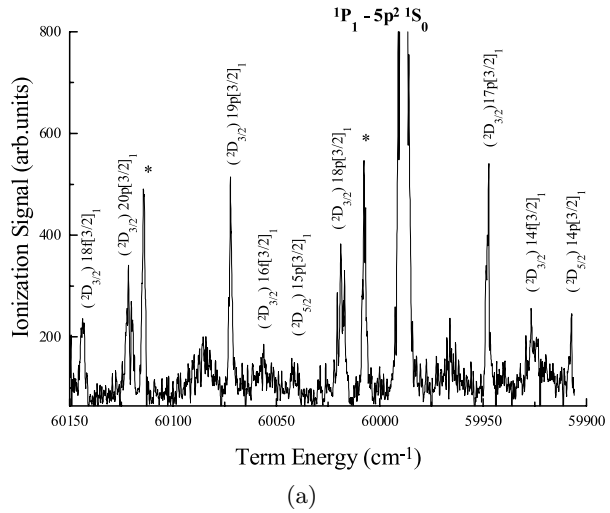

(a)

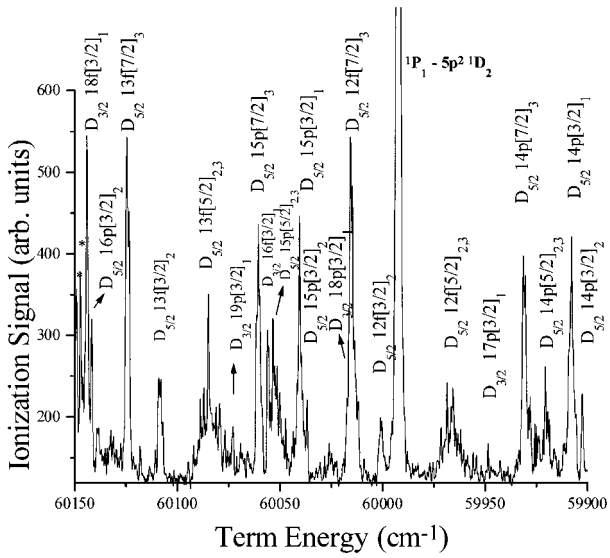

(b)

Fig. 2. (a) The spectrum of strontium below the $4d_{3/2}$ threshold excited from the $4d^2$ $^3P_0$ intermediate level showing the Rydberg series attached to the both ionic levels. The relative intensities of the series pertaining to the $4d(^2D_{5/2})n\ell$ configuration are worth noting. Only one Rydberg series $4d(^2D_{3/2})np$ $[3/2]_1$ have been observed attached to the $4d_{3/2}$ threshold. (b) The spectrum of strontium showing the structure excited from the $4d^2$ $^3P_2$ intermediate level. The relatively higher intensities of the series pertaining to the $4d(^2D_{5/2})n\ell$ configuration are worth noting. The Rydberg series $4d(^2D_{3/2})np$ $[3/2]_1$ attached to the $4d_{3/2}$ threshold are very weak in intensity.

threshold have been detected. The lower transition probabilities of these levels may be attributed to the Δj selection rule. In order to assign the level structure built on the $4d_{5/2}$ threshold, the observed groups of levels clearly follow the jK coupling scheme designations. Considering the multiplet around 59 950–59 900 cm^{-1}, the first sharp line with effective quantum numbers $\nu_{5/2}$ (mod 1) = 0.245 is assigned as $4d(^2D_{5/2})14p$ $[3/2]_2$ followed by a stronger line $\nu_{5/2}$ (mod 1) = 0.291 as $4d(^2D_{5/2})14p$ $[3/2]_1$, a weak line with $\nu_{5/2}$ (mod 1) = 0.37 and 0.38 as $4d(^2D_{5/2})14p$ $[5/2]_{2,3}$ and the strongest line with $\nu_{5/2}$ (mod 1) = 0.44 as $4d(^2D_{5/2})14p$ $[7/2]_3$. The very sharp line at 59 947.3 cm^{-1} is assigned as $4d(^2D_{3/2})17p$ $[3/2]_1$. The dominating line in this energy region (scanning laser energy = 15 470.4 cm^{-1}) is attributed to the sequential excitation from the $4s5p$ $^1P_1$ resonance level to the $5p^2$ $^1D_2$ level (term energy = 36 960.9 cm^{-1}). Adjacent to it the weak line with $\nu_{5/2}$ (mod 1) = 0.952 is assigned as $4d(^2D_{5/2})12f$ $[3/2]_2$ and the strong line at 60 014.4 cm^{-1} with $\nu_{5/2}$ (mod 1) = 0.064 as $4d(^2D_{5/2})12f$ $[7/2]_3$. At higher energies the structure is attributed to the multiplets built on the $4d_{5/2}np$ and $4d_{5/2}nf$ configurations. Thus all the expected $4d(^2D_{5/2})np$ and nf series have been observed and assigned except the $4d(^2D_{5/2})nf$ $[3/2]_1$ series reported by Garton and Codling [5]. The comparison of the data presented in Figures 2a and 2b clearly shows that only transitions built on the $4d_{3/2}$ parent ion level are observed when excited from the $4d^2$ $^3P_0$ level whereas, all the $J = 1$ lines are weak and the lines built on the $4d_{5/2}$ parent ion levels are dominant when excited from the $4d^2$ $^3P_2$ intermediate level.

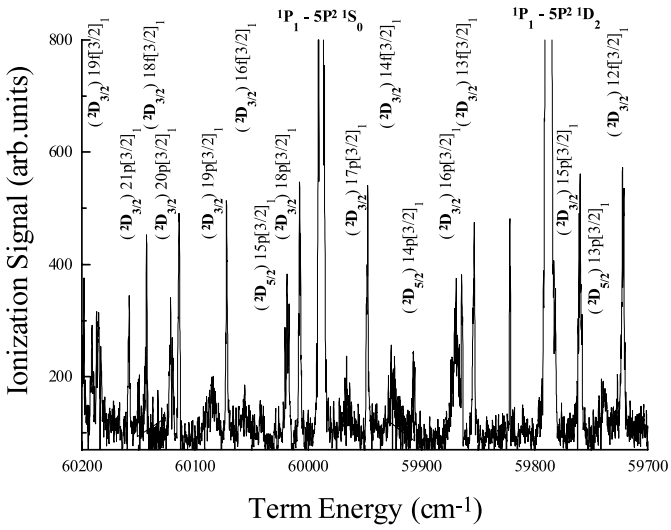

Fig. 3. The autoionizing resonances covering the energy region from 15 170 to 15 680 cm^{-1} excited from the $4d^2$ $^3P_0$ intermediate level. The dominating lines are attributed to the sequential excitation from the $5s5p$ $^1P_1$ level to the $5p^2$ $^1S_0$ and $5p^2$ $^1D_2$ levels respectively.

Figure 3 shows the over all view of the autoionizing resonances observed from the $4d^2$ $^3P_0$ intermediate level covering the excitation laser energy from 15 680 cm^{-1} to 15 170 cm^{-1}. The series attached to the $4d_{5/2}$ parent ion level remain much weaker as compared to the Rydberg series attached to the $4d_{3/2}$ limit. Since the upper level possess $J = 0$ and 1, these lines are identified as $4d(^2D_{3/2})nf$ $[3/2]_1$ $(12 \leq n \leq 19)$ and $4d(^2D_{3/2})np$ $[3/2]_1$ $(15 \leq n \leq 21)$, based on the

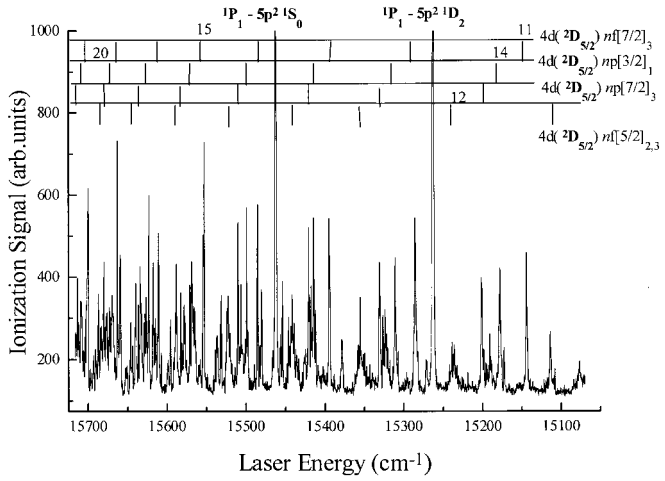

Fig. 4. The autoionizing resonances covering the energy region from 15 060 to 15 725 cm^{-1} excited from the $4d^2\ ^3P_2$ intermediate level. The dominating lines are attributed to the sequential excitation from the $5s5p\ ^1P_1$ level to the $5p^2\ ^1S_0$ and $5p^2\ ^1D_2$ levels respectively.

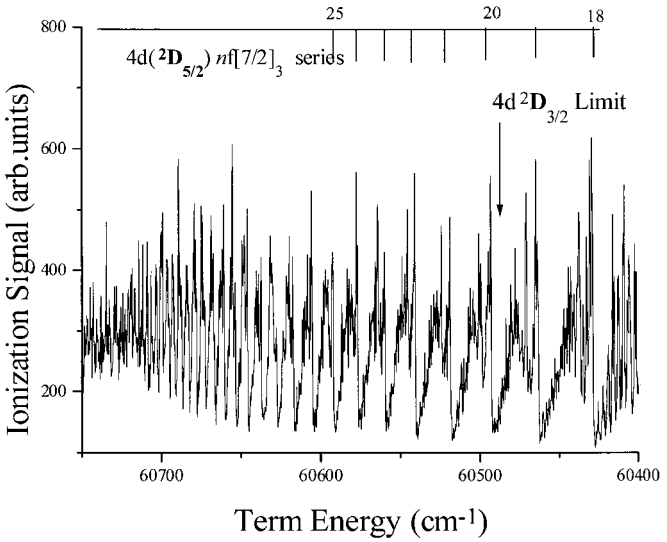

Fig. 5. The spectrum of strontium between the $4d_{5/2}$ and $4d_{3/2}$ thresholds covering the energy region between 60 750 to 60 400 cm^{-1} showing the autoionizing resonances.

known data [5]. The $4d(^2D_{5/2})np\ [3/2]_1$ $(13 \leq n \leq 15)$ lines remain too weak. The two dominating lines observed at the scanning laser energies at 15 262.7 cm^{-1} and 15 462.9 cm^{-1} are attributed to the sequential excitation as: $5s5p\ ^1P_1 \rightarrow 5p^2\ ^1D_2$ and $5s5p\ ^1P_1 \rightarrow 5p^2\ ^1S_0$ respectively.

Figure 4 shows the identifications of the autoionizing Rydberg series attached to the $4d_{5/2}$ limit excited from the $4d^2\ ^3P_2$ intermediate level covering the excitation laser energy from 15 725 cm^{-1} to 15 060 cm^{-1}. The stronger Rydberg series are assigned as $4d(^2D_{5/2})nf\ [7/2]_3$ $(11 \leq n \leq 18)$, $4d(^2D_{5/2})np\ [3/2]_1$ $(14 \leq n \leq 21)$, $4d(^2D_{5/2})np\ [5/2]_3$ $(14 \leq n \leq 21)$ and $4d(^2D_{5/2})nf\ [5/2]_{2,3}$ $(11 \leq n \leq 18)$ respectively in order of increasing energy. The sequentially excited levels, $5s5p\ ^1P_1 \rightarrow 5p^2\ ^1D_2$ and $5s5p\ ^1P_1 \rightarrow 5p^2\ ^1S_0$ are the dominant features in this region. The $4d_{3/2}$ ionization limit lies at the excitation laser energy 15 758.2 cm^{-1} (term energy = 60 488.1 cm^{-1}) and some of the high lying levels might have gained oscillator strength that explains the crowded structure around 15 650 cm^{-1}.

Figure 5 shows the autoionizing spectrum of strontium between the $4d_{5/2}$ and $4d_{3/2}$ ionization thresholds excited from the $4d^2\ ^3P_2$ intermediate level covering the energy region from 60 750 to 60 400 cm^{-1}. The arrow indicates the $4d(^2D_{3/2})$ limit. In this region, besides the $5s(^2S_{1/2})\varepsilon\ell$ channels a number of $4d(^2D_{3/2})\varepsilon\ell$ channels become available for the decay of the levels built on the $4d_{5/2}$ threshold. Inspecting the data in Figure 8 of Kompitsas *et al.* [12] between the $4d\ ^2D_{3/2}$ and $^2D_{5/2}$ thresholds, the $4d(^2D_{5/2})np$ ($\nu_{5/2}$ (mod 1) = 0.53) are broad and dominating in intensity as compared to a weak and broad $4d(^2D_{5/2})nf$ ($\nu_{5/2}$ (mod 1) = 0.10) and a much weaker and sharp $4d(^2D_{5/2})nh$ ($\nu_{5/2}$ (mod 1) = 0.99) series. The spectra observed in the present experiment differ considerably from that of Kompitsas *et al.* [12]. This difference is attributed to the fact that Kompitsas *et al.* [12] used the $4p^2\ ^1D_2$ intermediate level whereas, we have taken the $4d^2\ ^3P_2$ as intermediate level. Although both these intermediate levels possess the same J-value but they belong to different configurations and their K-values also differ. The MCHF calculations [26] show very strong mixing of the $5p^2$ and $4d^2$ configurations. Aspect *et al.* [26] remarked that the $4p^2\ ^1D_2$ level is only 35% pure and it contains 61% of the $4d^2\ ^1D_2$ level. Therefore, the spectra from both these intermediate levels, at least in the autoionizing region, are expected to be very similar. However, this is not what we have observed in the present experiment. We observed a strongest series that shows Fano-type [27] line shapes with a clear minimum in the cross-section and possess the effective quantum number $\nu_{5/2}$ (mod 1) = 0.02 assigned as $4d(^2D_{5/2})nf\ [7/2]_3$. The other two relatively broad series possess $\nu_{5/2}$ (mod 1) = 0.25 and 0.42 are assigned as $4d(^2D_{5/2})np\ [3/2]_{1,2}$ and $4d(^2D_{5/2})np\ [5/2]_{2,3}$ respectively. The series with $\nu_{5/2}$ (mod 1) = 0.75 and 0.82 are assigned as $4d(^2D_{5/2})nf\ [5/2]_{2,3}$ and $4d(^2D_{5/2})np\ [3/2]_2$ respectively. Thus, purely based on the quantum defects values it is noticed that the strongest series in the Kompitsas's data is the weakest in the present data and it also seems that the $4d(^2D_{5/2})np$ and nf $J = 1$ series are too weak to be detected.

All the newly observed levels lie above the first ionization threshold, and the broad structure associated to the $4d(^2D_{5/2})np$ states indicate a large coupling with the $4d(^2D_{3/2})\varepsilon\ell$ open channels whereas, the sharp ones for the $4d(^2D_{5/2})nf$ states show that the coupling is much smaller. In order to unveil the observed structure in the autoionizing region, we have selected an envelope of levels adjacent to the $4d_{3/2}$ limit (see Fig. 6) covering the region from 60 490 to 60 520 cm^{-1}. To simulate the

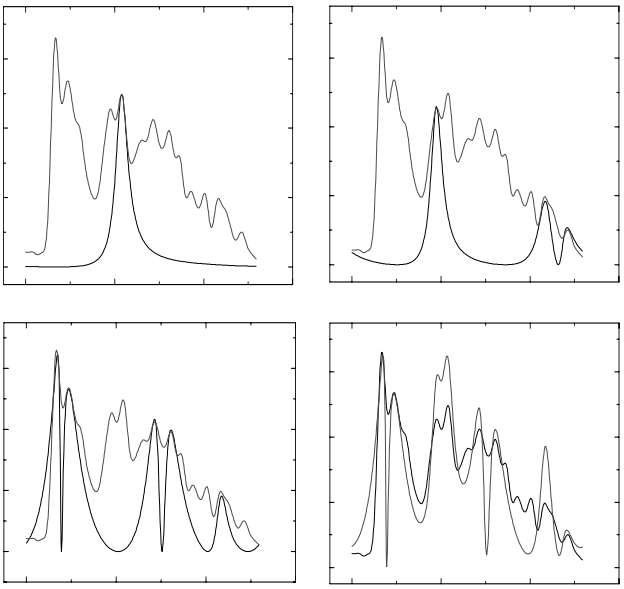

Fig. 6. (a) The experimental date and the simulated spectrum for $J = 1$ levels using a two-channel quantum defect theory model. (b) The experimental data and the simulated spectrum for $J = 2$ levels using a four-channel quantum defect theory model. (c) The experimental data and the simulated spectrum for $J = 3$ levels using a six-channel quantum defect theory model. (d) The experimental data and the sum of the $J = 1$, 2 and 3 levels simulated spectrum covering the energy region between 60 515 to 60 540 cm^{-1}.

observed spectrum, we have used the phase shifted multichannel quantum defect theory reaction matrix formulation of [28]. The MQDT equation in the matrix form is written as:

$$[\underline{R} + \underline{\varepsilon}]\,\underline{a} = 0 \tag{2}$$

where $\underline{R}$ is the interaction matrix with zero diagonal elements, the off diagonal elements R_{ij} describe the interaction between the ith and the jth channels and $\underline{\varepsilon}$ is the diagonal matrix whose components for the bound channels are given as:

$$\varepsilon_i = \tan\left[\pi\left(\nu_i + \delta_i\right)\right] \tag{3}$$

where δ_i are the quantum defects, ν_i are the effective quantum number of the ith bound channel with respect to the ith ionization threshold: $\nu_i = \sqrt{Ry/(IP - E_n)}$ and $\underline{a}$ is the column vector given by

$$a_i = A_i \cos\left[\pi\left(\nu_i + \delta_i\right)\right] \tag{4}$$

here A_i are the amplitudes of the ith dissociation channels. In the present studies, we have considered two channels, four channels and six channels models to simulate the spectra. A four channel MQDT compatibility equation is then written as:

$$\begin{vmatrix} \tan\left[\pi\left(\nu_1+\delta_1\right)\right] & R_{12} & R_{13} & R_{14} \\ R_{12} & \tan\left[\pi\left(\nu_2+\delta_2\right)\right] & R_{23} & R_{24} \\ R_{13} & R_{23} & \tan\left[\pi\left(\nu_3+\delta_3\right)\right] & R_{34} \\ R_{14} & R_{24} & R_{34} & \tan\left[\pi\left(\nu_4+\delta_4\right)\right] \end{vmatrix} = 0. \tag{5}$$

Within the framework of this model, we have derived a relation [29] that takes into account the interaction between a generalized one open channel, labeled 1 of the N channels, and the other $(N-1)$ closed channels. The photoionization cross-section given by Cooke and Cromer [28], Ueda [30] is represented in terms of cofactors [29]

$$\sigma = 4\pi^2\alpha\hbar\omega \frac{\left|\sum_1^N C_{1i}D_i\right|^2}{C_{11}^2 + \left|\sum_2^N C_{1i}R_{1i}\right|^2} \tag{6}$$

where $\hbar\omega$ is the photon energy which doesn't change appreciably over the small energy range considered by a typical single photon autoionizing spectrum and the short range parameters D_i are the transition dipole moments between the initial state and the ith channel and R_{1i} are the interchannel interaction parameters that correspond to autoionization of the discrete levels of channels 2, 3 and 4 in to the continuum and reflect the widths of these autoionizing resonances. The summation in the numerator is over all the N-channels involved and in the denominator the summation is only over the bound channels. The C_{1i} are the co-factors of the first row of the four channel MQDT matrix from equation (5). By substituting the co-factors one can calculate the cross-section for any number of closed channels interacting with one generalized open channel. Since the channel-1 is open which is attached to the $4d(^2\mathrm{D}_{3/2})$ ionization threshold and all the other channels are attached to the $4d(^2\mathrm{D}_{5/2})$ ionization threshold, therefore the open channel phase is represented as a function of the effective quantum number with respect to the second ionization threshold. The expression for the photoionization cross-section for two and three channels, after inserting the co-factors, turns out to be similar to the analytical expression derived by Giusti-Suzor and Lefebvre-Brion [31].

Since the envelop contains the contributions of $J = 1, 2$ and 3 levels and the multichannel quantum defect theory is applicable only for the same J-value levels, we have therefore simulated the contribution of the individual levels separately. We have identified only one series of $J = 1$ levels, three series of $J = 2$ levels and five series of $J = 3$. Figure 6a shows the experimental data along with the simulated spectra for $J = 1$ using a two channel model, one open and one closed. In Figure 6b the experimental data along with the $J = 2$ simulated spectra are shown using a four channel model, one open and three closed channels. In Figure 6c, the experimental data along with the $J = 3$ simulated spectra is shown using a six channel model, one open and five closed channels. By summing all these simulated spectra the resulting spectra is shown in Figure 6d along with the experimental data revealing an excellent

agreement. The MQDT parameters for the $4d(^2D_{5/2})np$, nf series for $J = 1$–3 are given below

$J = 1$

$R_{12} = 0.315 \quad D_1 = -2 \quad D_2 = 7 \quad \delta_1 = 0.755$

$J = 2$

$R_{12} = 0.30 \quad R_{13} = 0.34 \quad R_{14} = 0.300$

$D_1 = -0.1 \quad D_2 = 7 \quad D_3 = 4.5 \quad D_4 = 3$

$\delta_1 = 0.800 \quad \delta_2 = 0.330 \quad \delta_3 = 0.230$

$J = 3$

$R_{12} = 0.29 \quad R_{13} = 0.35 \quad R_{14} = 0.34$

$D_1 = -2 \quad D_2 = 7.3 \quad D_3 = 8$

$\delta_1 = 0.023 \quad \delta_2 = 0.98 \quad \delta_3 = 0.62$

$R_{15} = 0.34 \quad R_{16} = 0.3$

$D_4 = 7 \quad D_5 = 6.7 \quad D_6 = 4$

$\delta_4 = 0.550 \quad \delta_5 = 0.324.$

Figure 7 shows the simulated Rydberg spectra, sum of the $J = 1$, 2 and 3 levels, using the parameters determined from Figure 6 covering the energy from 60 750 to 60 400 cm^{-1}. This simulated spectra can be compared with the corresponding experimentally observed spectra shown in Figure 5. The agreement is excellent although we have used a much simplified MQDT model. The exact reproduction of the experimental profiles had not been possible because we have not considered a number of other close channels attached to the $4d_{5/2}$ threshold.

In conclusion, we have presented new data on the odd parity $J = 1$, 2 and 3 autoionizing Rydberg levels of strontium excited from the $4d^2\ ^3P_0$ and $4d^2\ ^3P_2$ levels. The level assignments have been made within the frame work of the jK-coupling scheme. It is observed that from the $4d^2\ ^3P_0$ intermediate level only the Rydberg levels attached to the $4d_{3/2}$ parent ion level and $J = 1$ are observable whereas, from the $4d^2\ ^3P_2$ intermediate level only the Rydberg levels attached to the $4d_{5/2}$ parent ion levels possessing $J = 2$ and 3 are observable, the $J = 1$ levels are too weak to be observed. The autoionizing resonances between the $4d_{3/2}$ and $4d_{5/2}$ thresholds are found to be dominated by the $4d(^2D_{5/2})\ nf$ series possessing the effective quantum number $\nu_{5/2} = 0.02$ in contrast to the strong autoionizing resonances with $\nu_{5/2} = 0.53$ observed by Kompitsas *et al.* [12] who used $4p^2\ ^1D_2$ as an intermediate level in the excitation scheme.

It is a great pleasure to acknowledge fruitful discussions on the subject and the pleasant hospitality of Prof. Dr. Demtroeder at Kaiserslautern University, Germany. We thank the AvH (Germany), TWAS Trieste, Pakistan Science Foundation PSF(104) and the PAEC (Pakistan) for providing the financial support. M. Yaseen and Raheel Ali are grateful to ICTP for providing scholarship under the ICAC scheme. MAB is thankful to the BMFT for financing the present visit to the Kaiserslautern University, Germany where the work was completed.

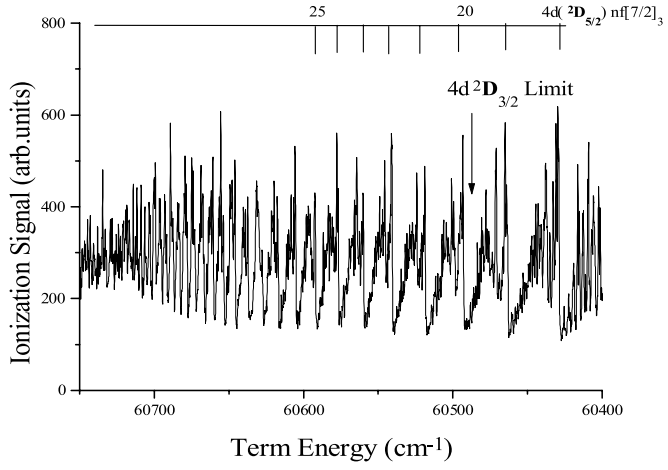

(a)

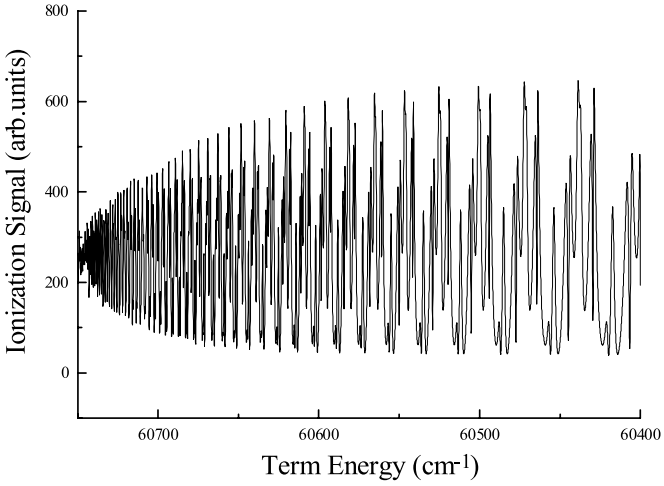

(b)

Fig. 7. The experimental and simulated spectrum of the autoionizing Rydberg series covering the energy region from 60 750 to 60 500 cm^{-1} using the parameters determined from the profiles shown in Figure 6.

References

1. J.P. Connerade, *Highly Excited Atoms* (Cambridge University Press, 1998)
2. W. Demtroeder, *Laser Spectroscopy* (Springer Verlag, Berlin, 1998)
3. T.F. Gallagher, *Rydberg Atoms* (Cambridge University Press, 1994)
4. V.S. Letokhov, *Laser Photoionization Spectroscopy* (Academic Press, Orlando, FL, 1987)
5. W.R.S. Garton, K. Codling, J. Phys. B **1**, 106 (1968)
6. R.D. Hudson, V.L. Carter, P.A. Young, Phys. Rev. **180**, 77 (1969)
7. J.P. Connerade, M.A. Baig, W.R.S. Garton, G. Newsom, Proc. Roy. Soc. A **371**, 295 (1980)
8. C.M. Brown, M.S. Longmire, M.L. Ginter, J. Opt. Soc. Am. **73**, 985 (1983)
9. M. Aymar, J. Phys. B: At. Mol. Opt. Phys. **20**, 6507 (1987)

10. C.H. Greene, Phys. Rev. A **28**, 2209 (1983)
11. C.H. Greene, Phys. Rev. A **32**, 1880 (1985)
12. M. Kompitsas, S. Cohen, C.A. Nicolaides, O. Robaux, M. Aymar, P. Camus, J. Phys. B: At. Mol. Opt. Phys. **23**, 2247 (1990)
13. M. Kompitsas, S. Goutis, M. Aymar, P. Camus, J. Phys. B: At. Mol. Opt. Phys. **24**, 1557 (1991)
14. S. Goutis, M. Aymar, M. Kompitsas, P. Camus, J. Phys. B: At. Mol. Opt. Phys. **25**, 3433 (1992)
15. A. Jimoyiannis, A. Bolovinos, P. Tsekeris, Z. Phys. D **22**, 577 (1992)
16. S.M. Farooqi, J.P. Connerade, M. Aymar, J. Phys. B: At. Mol. Opt. Phys. **25**, L219 (1992)
17. A. Jimoyiannis, A. Bolovinos, P. Tsekeris, P. Camus, Z. Phys. D **25**, 135 (1993)
18. C.J. Dai, J. Lu, J. Phys. B: **29**, 2473 (1996)
19. W.E. Cooke, T.F. Gallagher, S.A. Edelstein, R.M. Hill, Phys. Rev. Lett. **40**, 178 (1978)
20. E.Y. Xu, Y. Zhu, O.C. Mullins, T.F. Gallagher, Phys. Rev. A **33**, 2401 (1986)
21. E.Y. Xu, Y. Zhu, T.F. Gallagher, Phys. Rev. A **35**, 1138 (1987)
22. Y. Zhu, E.Y. Xu, T.F. Gallagher, Phys. Rev. A **36**, 3751 (1987)
23. U. Griesmann, B. Esser, J. Hormes, J. Phys. B: At. Mol. Clust. **27**, 3939 (1994)
24. M.A. Baig, M. Yaseen, R. Ali., A. Nadeem, S.A. Bhatti, Opt. Commun. **156**, 279 (1998)
25. C.E. Moore, *Atomic Energy Levels* (NBS Circular No 35, Washington DC, 1971), Vol. 2
26. A. Aspect, J. Bauche, A.L.A. Fonseca, P. Grangier, G. Roger, J. Phys. B: At. Mol. Opt. Phys. **17**, 1761 (1984)
27. U. Fano, Phys. Rev. A **15**, 1920 (1961)
28. W.E. Cooke, C.L. Cromer, Phys. Rev. A **32**, 2725 (1985)
29. M.A. Baig, S.A. Bhatti, Phys. Rev. A **50**, 2750 (1994)
30. K. Ueda, Phys. Rev. A **35**, 2484 (1987)
31. A. Giusti-Suzor, H. Lefebvre-Brion, Phys. Rev. A **30**, 3057 (1984)